Master Thesis

Friction stir butt welding of AA6061-T6: the effect of post-weld heat treatment

on

microstructures and mechanical properties

The Graduate School of the University of Ulsan

School of Mechanical Engineering

Van Cong Phan

Master Thesis

Friction stir butt welding of AA6061-T6: the effect of post-weld heat treatment

on microstructures and mechanical properties

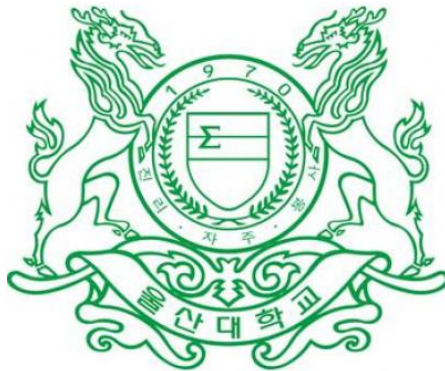The Graduate School of the University of Ulsan

School of Mechanical Engineering

Van Cong Phan

Friction stir butt welding of AA6061-T6: the effect of post-weld heat treatment on microstructures and mechanical properties

Advisor: Professor Sung-Tae Hong

A Thesis

Submitted to the Graduate School of the University of Ulsan

In partial Fulfillment of the Requirements

For the Degree of Master of Science

By

Van Cong Phan

School of Mechanical Engineering

Ulsan, Korea

June 2023

Friction stir butt welding of AA6061-T6: the effect of post-weld heat treat-

ment on

microstructures and mechanical properties

This certifies that the thesis of Van Cong Phan is approved.

Committee Chair Professor Doo-Man Chun

Committee Member Professor Sung-Tae Hong

Committee Member Professor Jin-Woo Lee

School of Mechanical Engineering

Ulsan, Korea

June 2023

ACKNOWLEDGMENT

First and foremost, I would like to express my sincere gratitude to Professor Sung-Tae Hong for his enthusiasm and immense knowledge. His guidance helped me in all aspects of research and writing this thesis. I feel fortunate to have had the opportunity to work under his guidance during my graduate studies.

I appreciate all my fellow labmates in the Advanced Engineering Materials Laboratory. Especially, Do Thanh Thuong, Bui Thi Tu Anh, and Soumyabrata Basak enlightened me with the first glance of research, supporting me in my daily life, engaging in stimulating discussions, and for all the fun we have had over the last two years.

In addition, I would like to express my gratitude to all the employees and Professors at the School of Mechanical Engineering, University of Ulsan, for their excellent work.

Last but not least, I would like to express my deep gratitude to my family, who have always been by my side and supported each of my decisions. Their support accelerated my motivation, which helped me overcome the difficulties and complete my master's course.

ABSTRACT

This study investigates the effect of post-weld heat treatment (PWHT) on the mechanical properties of friction stir welded (FSW) AA6061-T6 aluminum alloy. The microstructure and precipitation behavior in the stir zone has been characterized by optical microscopy (OM), scanning electron microscopy (SEM), followed by an Energy-Dispersive Spectroscopy (EDS), and Electron Backscatter Diffraction (EBSD) analysis. SEM and EDS analyses confirm that mechanical properties improved due to the re-precipitation and dispersion of fine precipitates in the heat-treated FSW joint. EBSD maps reveal recrystallized ultra-fine grain structures (2.44 μm) inside the SZ. In addition, the abnormal growth grain phenomenon and bimodal structure during post-weld heat treatment were present in the stir zone, simultaneously with significant grain size growth (125.54 μm). The tensile test and microhardness results show that the joint has superior mechanical properties after heat treatment than the as-fabricated joint (no heat treatment). It should be noted that the fracture surface of both the PWHT and FSW joints exhibited ductile fracture mechanisms.

Keywords: Friction stir welding, Aluminum alloy, Heat treatment, Microstructure analysis, Mechanical properties.

TABLE OF CONTENTS

LIST OF FIGURES

LIST OF TABLES

1. INTRODUCTION

1.1. Overview of the trend of lightweight material and 6061-T6 Aluminum alloy

The current imperatives of climate change, resource scarcity, and market growth are necessitating the development of efficient and economical manufacturing processes for automotive products. As a result, lightweight material has emerged as an integral approach to enable sustainable, low-energy solutions across various industries. In addition, advances in materials science and manufacturing processes are making it increasingly possible to use lightweight materials in broader applications [1]. In several industries, including aerospace, automotive, and construction, aluminum alloys are regarded as one of the foremost critical lightweight materials. Due to its exceptional properties, including its lightweight nature, high strength-to-weight ratio, excellent corrosion resistance, good conductivity, and machinability, aluminum alloy has gained popularity as a material of choice. However, some of its drawbacks are its low melting point, poor wear resistance, low strength, and is significantly more expensive than other materials [2]. Therefore, aluminum alloys were divided into series based on the elemental composition and desired properties. The AA6xxx series, in which magnesium and silicon are the principal alloying elements, is required to form magnesium silicide (Mg_2Si). The typical type of this group is AA6061, which contains more than 1.5% magnesium combined with silicon and other additives such as Cu, Zn, and Cr. Adding magnesium and silicon in AA6061 contributes to its high strength and corrosion resistance. Magnesium increases the alloy's strength by forming a solid solution with aluminum, while silicon increases corrosion resistance by forming an oxide film on the surface of the metal. The other elements, such as iron and copper, also enhance the material's properties, contributing to its strength and chromium providing additional corrosion resistance. AA6061-T6 is a heat-treated aluminum alloy that involves solutionizing the material at high temperatures, rapidly quenching it, and aging it at a lower temperature to

7

enhance its mechanical properties. It has outstanding properties making it an attractive material for numerous applications [3,4].

1.2. Overview of welding and Friction stir welding.

Welding is a critical method in the production of aluminum-based products. Fusion welding, in particular, plays a significant role in fabricating metallic structures. There are several types of fusion welding, such as gas tungsten arc welding (GTAW or TIG), gas metal arc welding (GMAW or MIG), and resistance spot welding (RSW). These methods use different heat sources, such as arc or electric, to melt the base material and create a bond between the two pieces. Although there are utilities, fusion welding has several limitations that must be considered the negative impact on joint quality. Heat input during a welding process can result in warping and cracking of the material, weakened structure, over-aging, and brittleness. In addition, gases like hydrogen and oxygen can lead to porosity within the weld and affect its quality. Welding of dissimilar metals can also prove challenging. Moreover, fusion welding can result in surface roughness and discoloration, adversely impacting the appearance and corrosion resistance of the structure [5]. FSW was invented in 1991 and emerged as an incredibly productive solid-state joining technique with several advantages for metal manufacturing. A non-consumable spinning tool is inserted inside the welded material, generating frictional heat and plastic deformation and joining the material without melting. FSW provides many advantages over conventional fusion welding methods, including improved joint strength, fatigue performance, reduced thermal distortion, versatility, and environmental friendliness. The FSW process produces more robust and uniform joints with minimal porosity or distortion. It can be used to join various materials, including those that are difficult to weld using traditional methods. The positive aspects of FSW's environmental friendliness, such as the lack of grinding waste, consumables like rods, wires, and fillers, shielding gases, the absence of smoke, pollutants, and

radiation, and the variety of material combinations, make it a desirable option in green and sustainable industry sectors [6,7,8].

FSW offers numerous advantages for metal fabrication; however, obtaining a high-quality joint of AA6061-T6 through this process remains challenging. According to Zhang et al. [9], the presence of oxide on the surface, which was broken owing to inadequate shearing under high welding speeds and low heat inputs, may result in "S" flaws in the weld nugget zone. As a result, the joint strength is diminished. Moreover, the microhardness is dramatically decreased, particularly in the heat-affected zone (HAZ) and thermo-mechanically affected zone (TMAZ), with reported reductions of up to 40% compared to the base material [10]. The heat generated during welding is predominantly attributed to the frictional forces between the workpiece and the tool shoulder. It causes localized heating that softens the material and allows the tool to travel through it, creating a bond. The amount of heat generated depends on several factors, such as the tool's rotating speed, the pressure applied, and the material being welded. During welding, the material's temperature could rise to 80% of its melting point [5,11]. It is typically maintained at temperatures ranging from 300°C to 550°C, corresponding to the HAZ and SZ. Furthermore, temperatures higher than 502°C caused the complete dissolving of precipitates to α-Al solid solution and adversely affected joint properties [12,13].

1.3. Overview of Post-weld heat treatment of aluminum alloy.

Numerous endeavors have been undertaken to improve the reliability of joins produced during friction stir welding (FSW), the most significant of which is applying the post-weld heat treatment (PWHT) method. Solution heat treatment and aging are typically the two steps of the heat treatment procedure for FSW joints. The former stage aims to dissolve any precipitates formed during welding, promote a homogeneous microstructure, reduce residual stresses, and improve joint ductility and toughness. The latter stage promotes the precipitation of new phases,

such as Mg2Si, to enhance joint strength and hardness while maintaining ductility. The impact of PWHT on mechanical characteristics and microstructure changes has been the subject of several investigations. For example, Baghdadi et al. [14] conducted a study on the influence of post-weld heat treatment on the mechanical characteristics of the AA6061 FSW joint. The joint efficiency was observed to drop to 65% of the base metal tensile strength, and a serrated flow behavior known as the Portevin-Le Chatelier (PLC) effect occurred in the FSW joint. T6-heat treatment was discovered to eliminate the PLC effect and restore the original mechanical characteristics of the FSW joint. It was attributable to the Mg2Si particles' superior dispersion, which enhanced precipitation hardening and minimized the growth of grains while boosting dislocation density as a result of applied strain. C. Rajendran et al. [15] investigated the effects of PWHT on the mechanical properties and microstructure of friction stir welded butt joints of AA2014-T6 aluminum alloy. They reported an improvement in the tensile strength and microhardness, along with an increase in the size of grains in all regions and abnormal grain growth (AGG) phenomena occurring in the SZ. This phenomenon was also found in İpekoğlu et al.'s investigation [16], which reported the influence of both annealed (O) and age hardening (T6) conditions on microstructural evolution. PWHT brought about a significant improvement and uniform microhardness distribution for both joints; however, the microhardness was not significantly impacted by the formation of AGG. Pabandi et al. [17] performed FSW on various AA2026-T6 and AA6061-T6 joints and found that following heat treatment, joint efficiency rose from 59% to 74% and 82.5% for AA6061 alloy on the retreating and advancing sides, respectively. Furthermore, fine precipitation of the (Mg2Si) phase was found in the HAZ of the AA6061 side, which increased the tensile strength and microhardness of the joint due to dispersion hardening effects [18]. The presence of particles acts as obstacles to dislocation movements resulting in enhanced resistance to plastic deformation, strength, and hardness. The precipitation of the hardening particles is typically achieved through artificial aging. To achieve

superior durability and toughness, the process includes heating the material at an appropriate temperature for a predetermined amount of time, followed by quenching and artificial aging [19]. However, a delay period is usually inevitable in commercial processing, known as "delay-aging" or "two-step aging" behavior. It is shown that cluster formation during natural aging, which does not transition into β" phase, has a detrimental impact leading to a low number density of precipitates and a decline in strength [20,21].

1.4. Objective

Currently, the impacts of PWHT on the FSW joint of AA6061-T6 are the subject of numerous research. However, there has been minimal research to understand the effect of two-step aging and intricate changes in microstructure related to mechanical properties. Therefore, the objective of this study is to determine the influence of PWHT followed by natural and artificial aging on the microstructural characteristics and establish microstructural changes correlation with mechanical properties of AA6061-T6 FSW joints.

2. METHOD

2.1. Processing

This study selected a commercial AA6061-T6 aluminum alloy of 150 mm x 100 mm x 3 mm as the base metal for overall experiments. The main chemical composition of the material is exhibited in Table 2.1. The butt joints were fabricated along the length of the sheets using the FSW machine, as shown in Figure 2.1 (RM-1, Bond Technologies, Elkhart, IN, USA), in the path of joining corresponding to the rolling direction, as depicted in Figure 2.2.
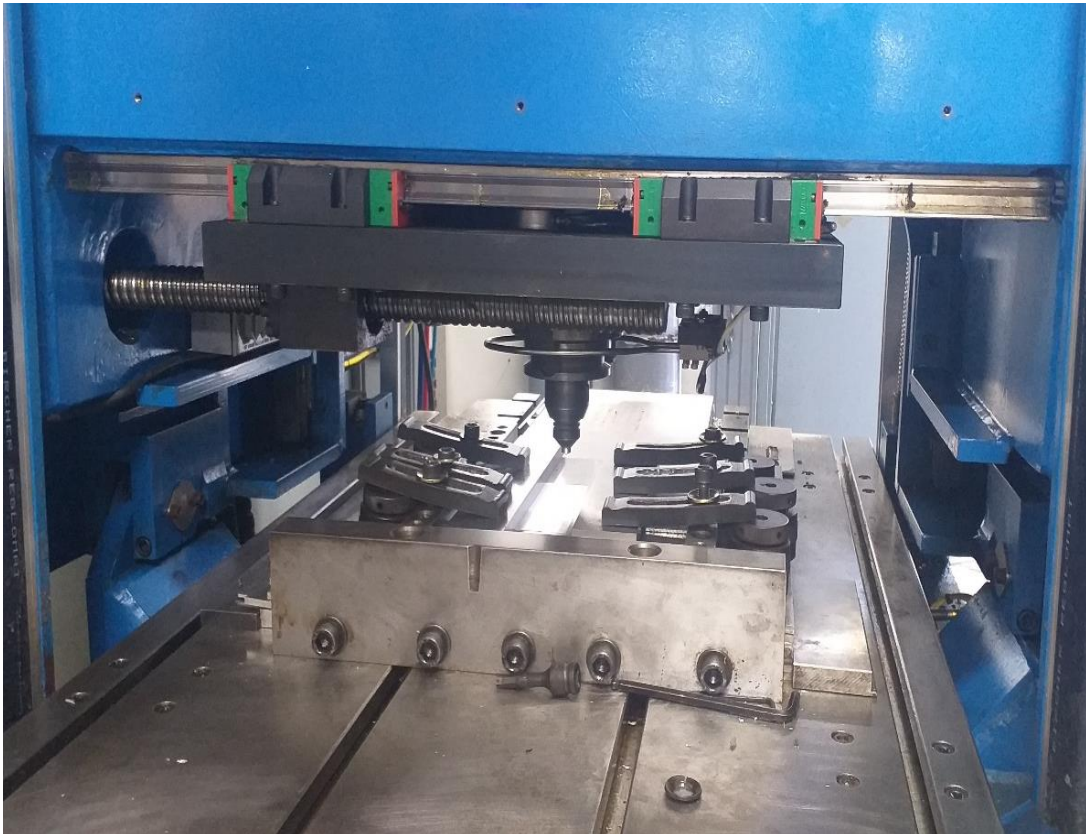
Figure 2.1 The experimental setup with a clamping system.

Table 2.1 Chemical compositions of AA6061-T6 (wt.%)

Materials	Si	Fe	Cu	Mn	Mg	Cr	Ni	Zn	Ti	Al
AA6061-T6	0.60	0.35	0.28	0.15	1.00	0.20	0.02	0.003	0.15	Bal.

(a)

(b)

(c)
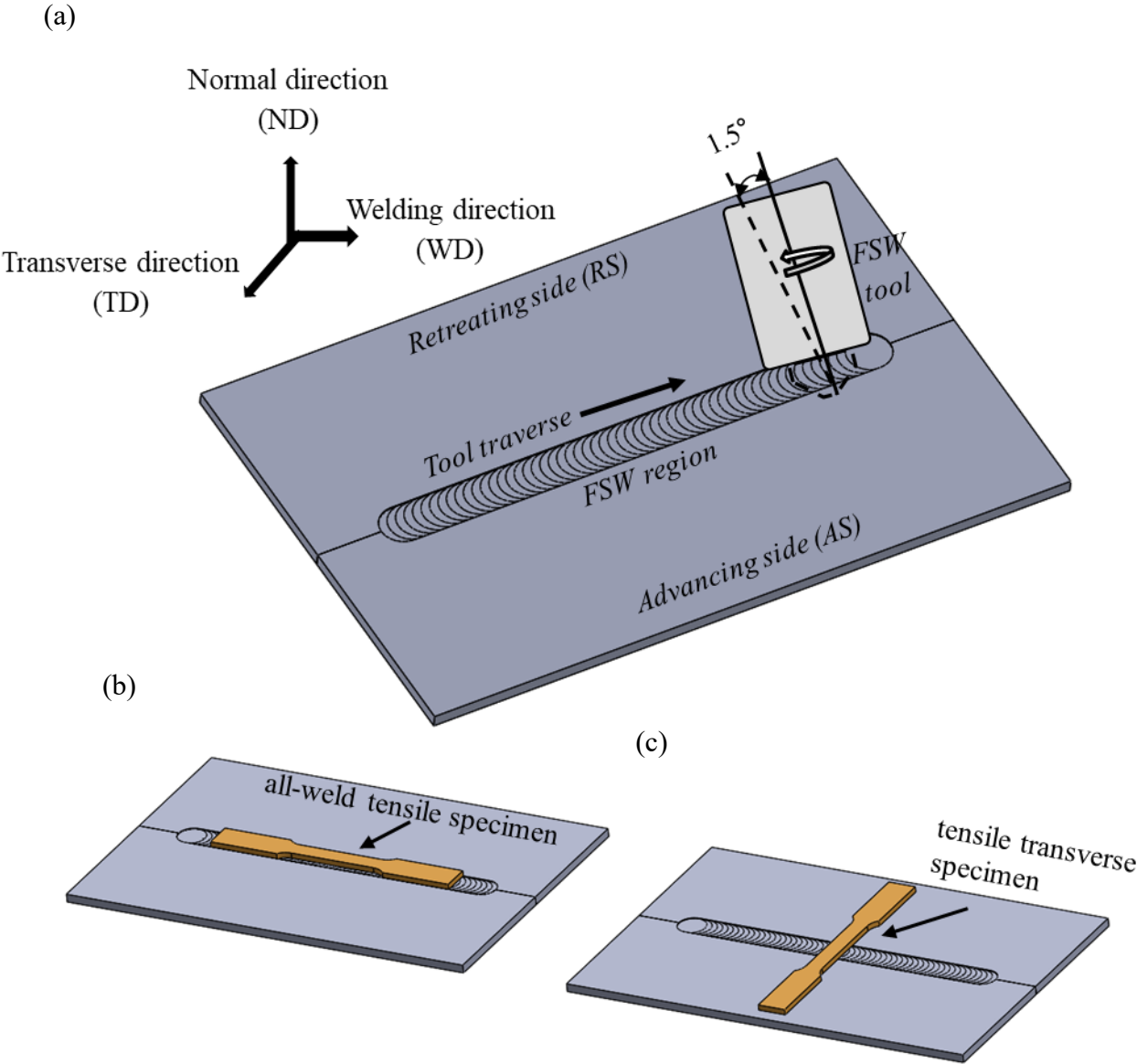
Figure 2.2 Schematic illustration of (a) butt FSW process of AA6061-T6 sheets, (b) all-weld, and (c) transverse tensile specimen fabrication.

Throughout this study, an H-13 steel tool with a concave shoulder was employed, and its geometry is shown in Table 2.2. Prior to conducting the subsequent experiment, a preliminary

tensile test of the joint was performed to determine an appropriate parameter, as indicated in Table 2.3. Following that, two separate sets of joints were divided between studying the influence of post-weld heat treatment: one as-welded sample and one heat-treated sample. The PWHT procedure, as illustrated in Figure 2.3, included solutionizing at 530°C for 1 hour, natural aging at ambient temperature for 24 hours, and artificial aging at 180°C for 4 hours.

Table 2.2 Tool geometry.

Material	H - 13 steel
Shoulder Diameter	10 mm
Shoulder shape	Concave
Pin diameter	3 mm
Pin type	Taper, threaded

Table 2.3 Welding process parameters.

Processing conditions	Tool rotational speed (rpm)	Welding velocity (mm/min)	Depth of penetration (mm)	Tool tilt angle (º)
Linear (Butt)	600	100	2.8	1.5
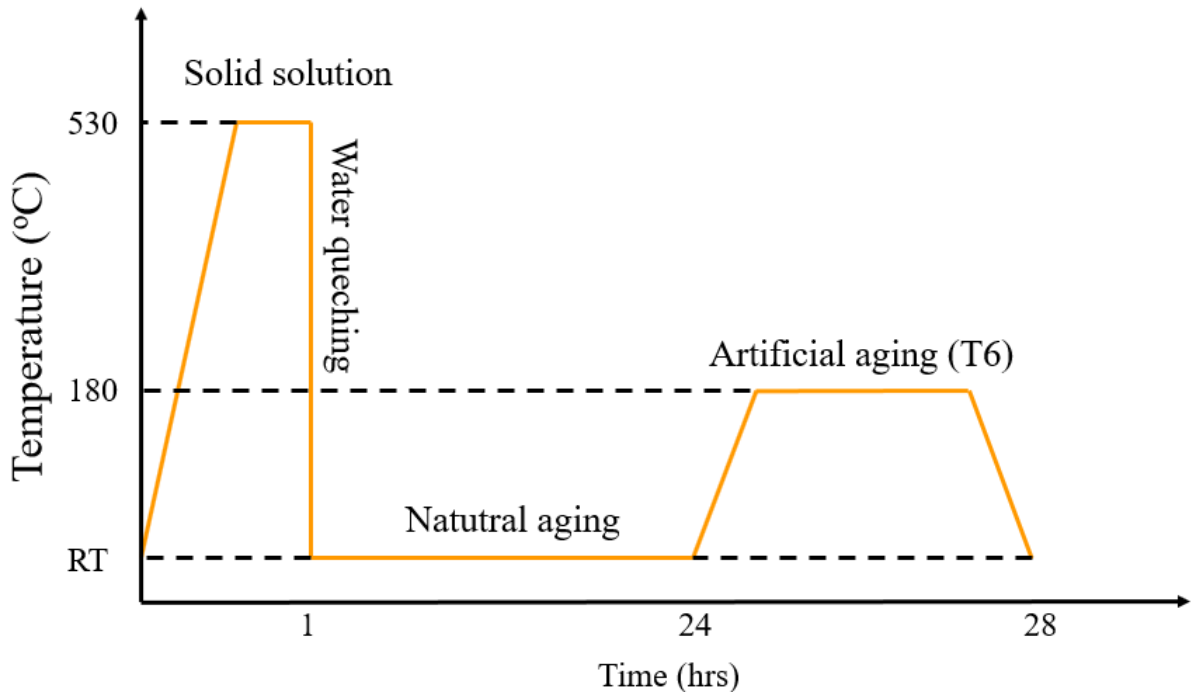
Figure 2.3 Diagrammatic representation of the heat treatment procedure.

2.2 Microstructural characterization

The joint cross-section was machined perpendicular to the weld direction (WD), subsequently ground, and polished to a surface roughness of approximately 1 μm using colloidal silica polishing suspension. Keller's reagent was used for optical microscopy (OM) (GX41, Olympus Corp., Tokyo, Japan) to etch the prepared surface. Field emission scanning electron microscopy (FE-SEM) (SU5000, Hitachi, Japan) equipped with energy-dispersive X-ray spectroscopy (EDS) (XMax50, HORIBA Ltd., Kyoto, Japan) was employed to investigate the formation of precipitates during friction stir welding and post-weld heat treatment, along with their chemical compositions in the base metal and the stir zone (SZ). For electron backscatter diffraction (EBSD) samples, the joint cross-section was further polished with a colloidal silica suspension of approximately 0.03 μm. The microstructural changes in the SZ of the FSW and PWHT joints were comprehensively characterized by obtaining inverse pole figure (IPF), grain boundary character distribution (GBCD), and Kernel Average Misorientation (KAM). IPF-

generated maps of the crystallographic orientation of individual grains allow us to understand the texture and the presence of grain boundaries and defects in a material. KAM measures the average misorientation between adjacent crystallographic orientations within a material, which can help identify regions of high deformation or plastic strain. The GBCD describes the frequency and distribution of different types of grain boundaries in a material based on their crystallographic orientation relationships. The misorientation between the two neighboring grains is used to create a color-coded map that indicates the frequency and distribution of different types of grain boundaries within the material. Grain identification was performed by setting a grain tolerance angle of 5°, with low-angle grain boundaries (LAGBs) between 2° and 15° and high-angle grain boundaries (HAGBs) fixed at angles greater than 15° (up to 180°).

2.3 Mechanical testing

In this study, microhardness mapping was carried out to determine the hardness distribution of a joint cross-section in the transverse direction (TD). Numerous point indents were applied uniformly on the entirety of the surface with a load of 0.49 N along with a dwell duration of 10 s using an automated Vickers microhardness tester (AMT-X7FS series, Matsuzawa, Japan). The hardness profile was examined for the center line of the weld cross-section, and the resulting profile was exhibited in relation to the surface microhardness mapping.

By using sub-size tensile specimens made all-weld tensile specimens in accordance with ASTM E8M04 standards, the tensile strength of the FSW joint was evaluated mechanical properties further. A universal testing apparatus (DTU900-MH, Daekyung Co., Ltd., Busan, South Korea) was employed to examine the specimens under uniaxial tensile conditions until fracture. Three samples from each category (BM, FSW, and PWHT joints) were evaluated to ensure the reliability of the results obtained. The transverse tensile specimens were subsequently placed through further testing to demonstrate a strong joining. Following that, Scanning Electron

Microscopy (SEM) was implemented to determine the characteristic fracture surfaces for investigating the underlying failure mechanism.

3. RESULTS AND DISCUSSION

3.1. Microstructural analysis

3.1.1 Optical microscopy and SEM analysis

The cross-section of the FSW and PWHT joints was examined using a low-magnification optical microscope, as shown in Figure 3.1. It was found that the FSW joint consists of the base metal (BM), the thermo-mechanically affected zone (TMAZ), and the stir zone (SZ) with a typical basin shape. Even distinct regions are no longer readily apparent after heat treatment. No macro-defects were observed in the stir zone. Furthermore, the combination of linear and rotational motion of the tool generates vortex flow, which causes the material to flow radially and tangentially around the probe, particularly in the bottom area of the stir zone [22].
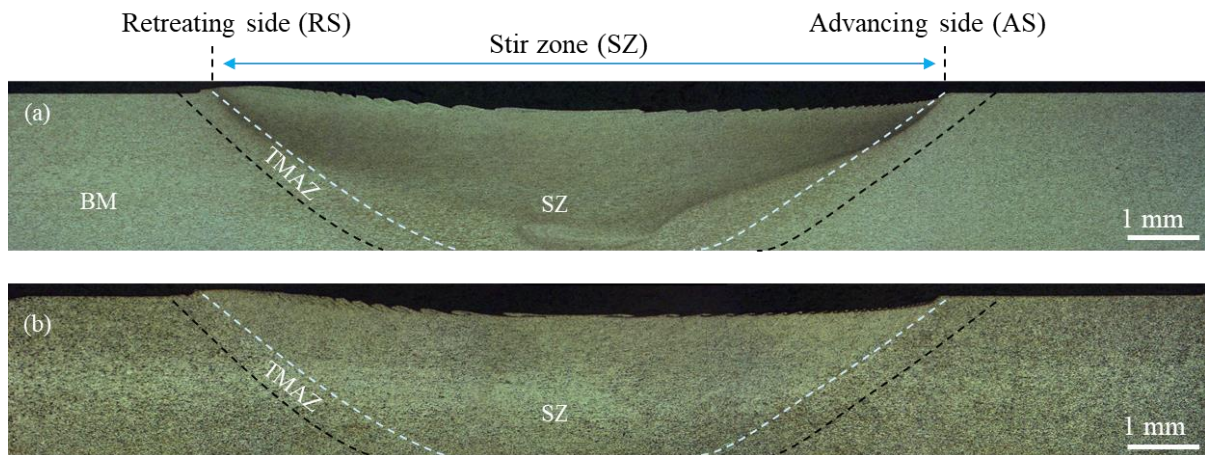
Figure 3.1 Macrograph of the AA6061-T6 cross-section showing various regions of (a) the FSW and (b) PWHT joints.
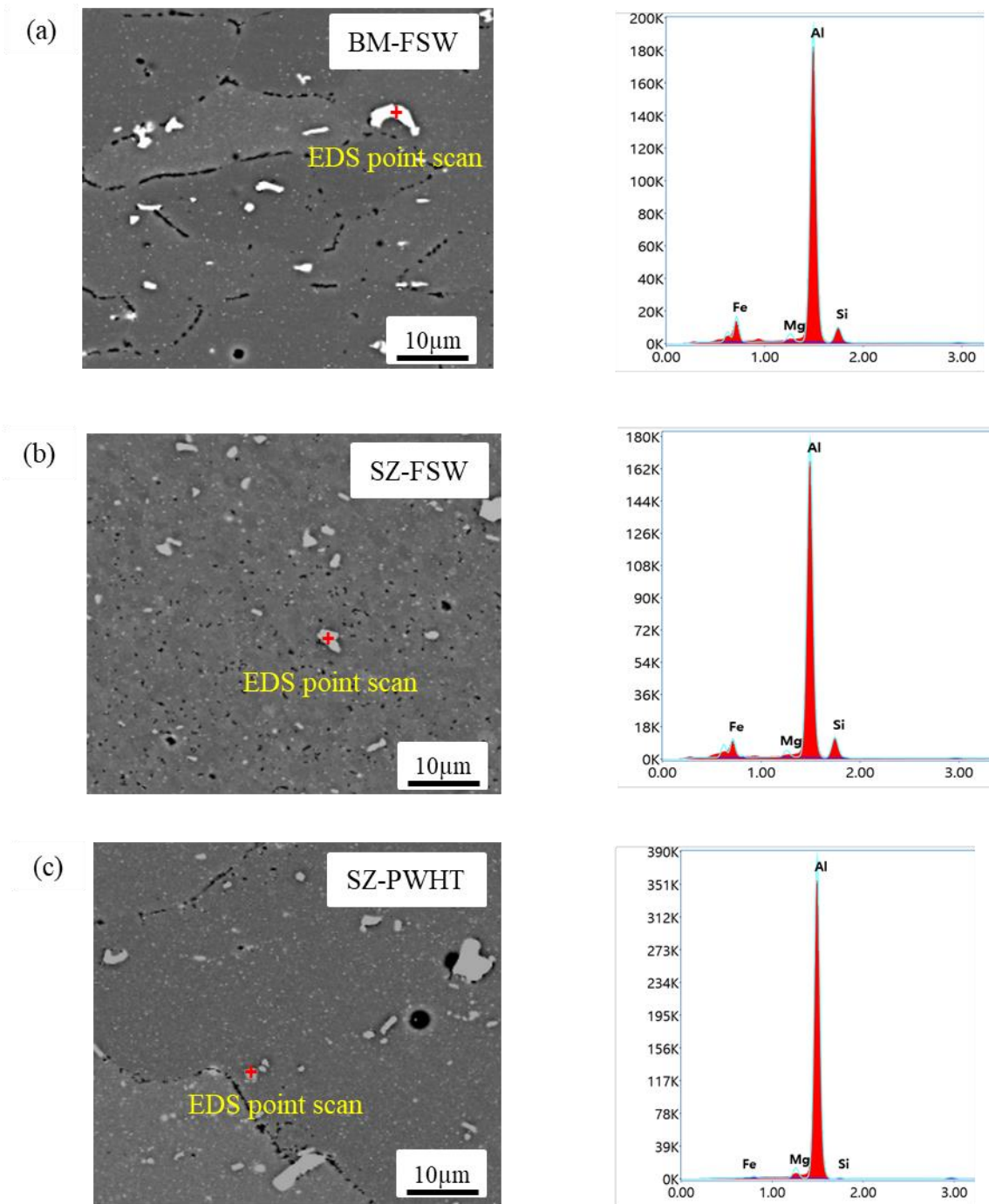
Figure 3.2 SEM/EDS point scan images showing the precipitate in (a, b) the BM and SZ of the FSW and (c) the SZ of the PWHT joints

The precipitates were identified by analyzing their chemical compositions using an SEM/EDS point scan technique, as illustrated in Figure 3.2. The Al-Mg-Si-Fe rich precipitates were present in all regions of the FSW joint. After heat treatment, re-precipitation was observed with the phase of Al-Mg-Si, particularly along the grain boundary and grain boundary junction.

Furthermore, nano precipitates were observed inside the grains. The heat treatment process causes existing precipitates to dissolve, followed by producing new precipitates from the dissolved material after the process has cooled. Because of the heat input and mechanical deformation during the welding process, the alloying elements in AA 6061 dissolve into a solid solution. As the alloy cools down, the solubility of the alloying components in the solid solution decreases. It leads to the formation of precipitates of the alloying components in the solid solution. These precipitates are formed because the alloying components have exceeded their solubility limit and are now insoluble in the solid solution. However, these precipitates are not fully developed and may not provide the desired strength and other properties. The post-weld heat treatment process helps to re-dissolve these precipitates and allow the alloying elements to re-distribute uniformly. This redistribution results in the formation of new grains, more defined precipitates that contribute to the required hardness and strength [23]. The regions with a higher concentration of defects, such as grain boundaries and grain boundary junctions, tend to favor the formation of new precipitates attributed to the presence of more vacancies, which facilitate atom diffusion. Moreover, these regions often act as diffusion paths, further promoting the formation of new precipitates [24].

3.1.2. EBSD analysis
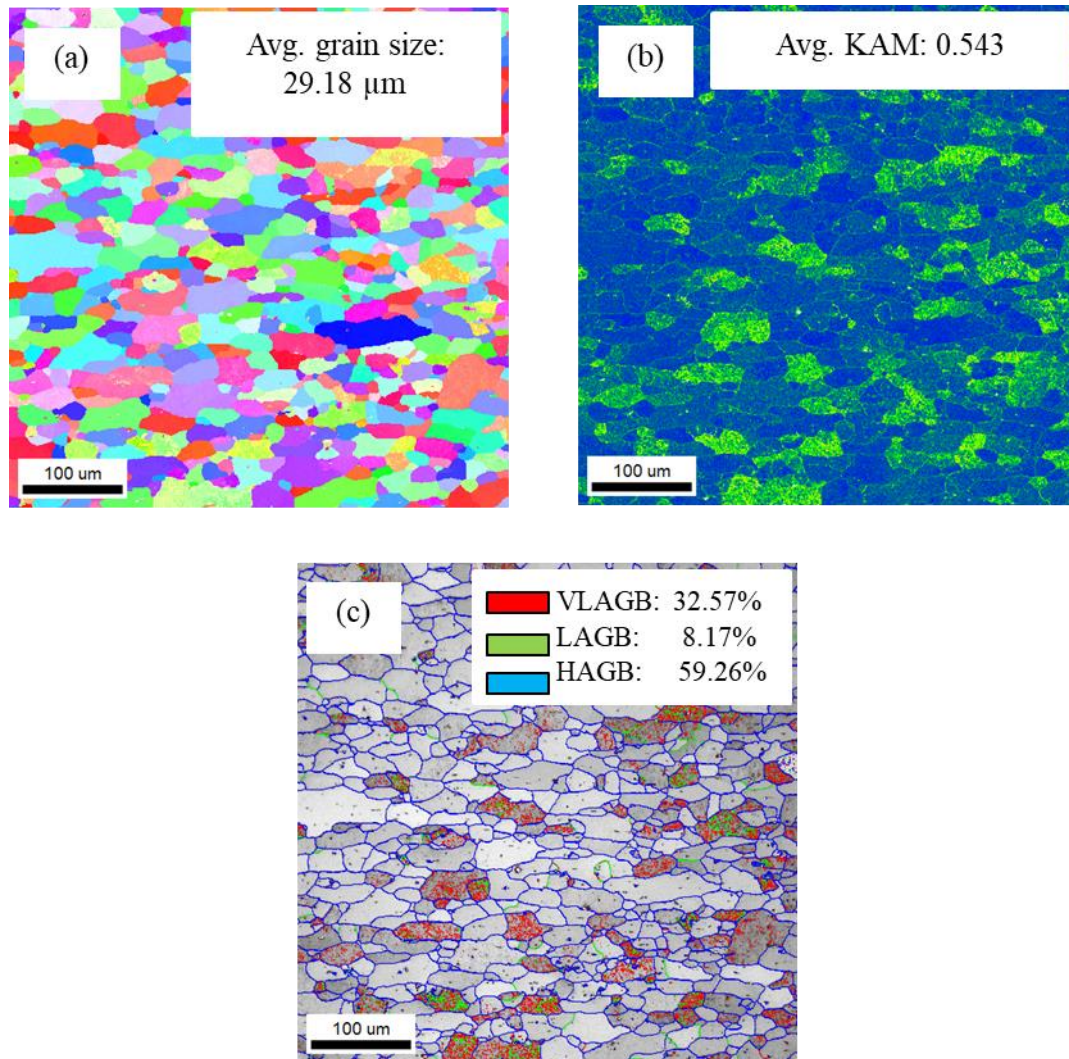
Figure 3.3 EBSD analysis: (a) IPF map, (b) KAM map, (c) GBCD map in the BM of the FSW joint.

In the BM of the FSW joint, the IPF map reveals an equiaxed recrystallization coarse grain structure with an average grain size of 29.18 μm (Figure 3.3(a)). There are slight differences between the proportions of HAGBs (blue lines, 59,25%) and LAGBs (red and green lines, 40.75%), as illustrated in Figure 3.3(c). Most LAGBs, on the other hand, were represented as red lines inside coarse grains, which was caused by the existence of sub-grains. It also can be explained by combining the KAM map, which describes the locally accumulating misorientation with a KAM value of 0.543 degrees, as shown in Figure 3.3(b).
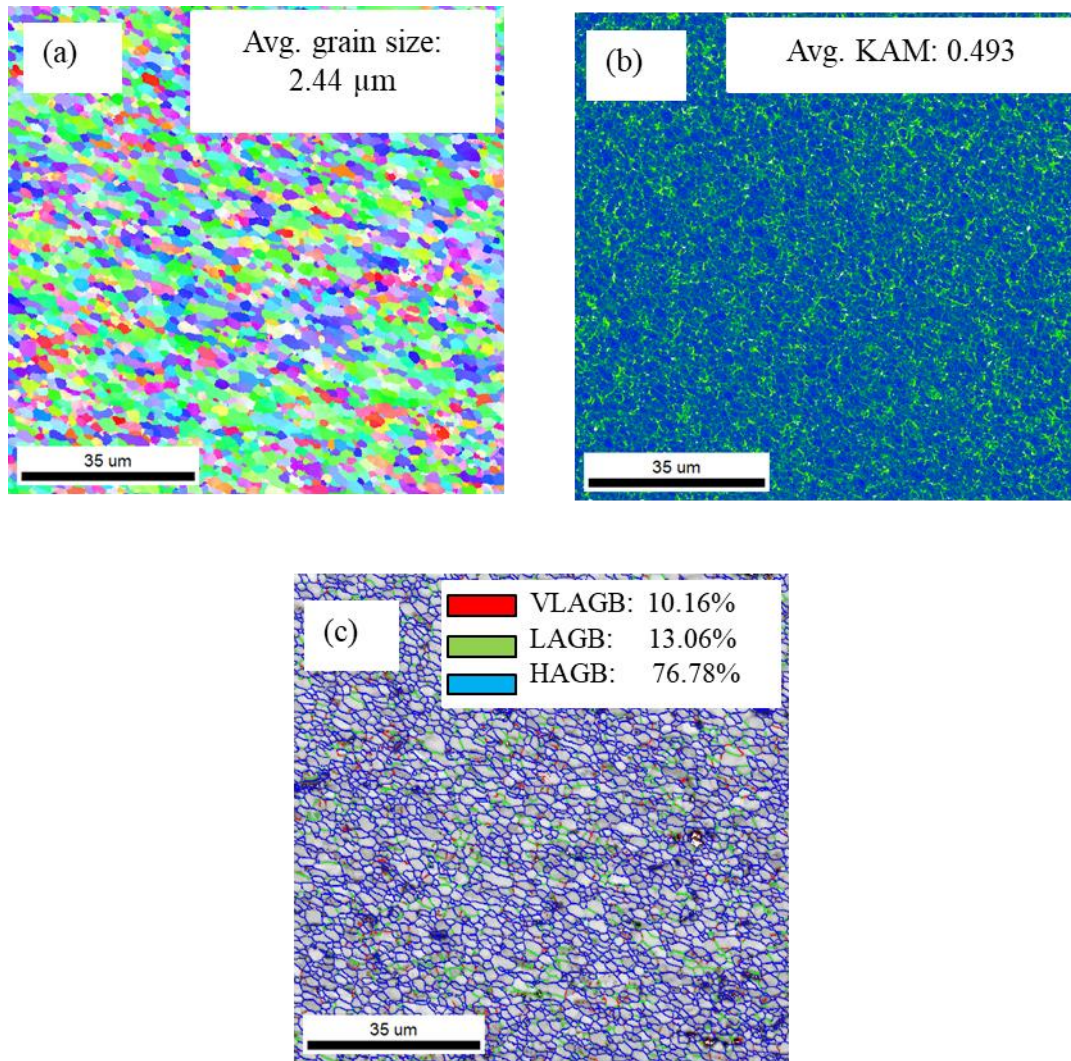
Figure 3.4 EBSD analysis: (a) IPF map, (b) KAM map, (c) GBCD map in the SZ of the FSW joint.

The microstructural evolution in the SZ caused by intense plastic deformation and heat generated by friction is shown in Figure 3.4. The average grain size of 2.44 m is shown by the IPF map of the SZ, which also demonstrated a continuous dynamic recrystallized (CDXR) fine grain structure, as illustrated in Figure 3.4(a) [6]. The GBCD map shows that the HAGBs (76.83%) outweigh the LAGBs (23.17%), as described in Figure 3.4(c). A fine and equiaxed grain structure is formed by the high strain rates and heats in the SZ, accompanied by dynamic recrystallization, which results in the formation of new grains and the elimination of pre-existing grains, leading to a high density of HAGBs in the microstructure. The SZ KAM map represents the distribution of intergranular dislocations, which occur through the reconstruction of

dislocations and other defects during plastic deformation and recrystallization, as shown in Figure 3.4(b). The average KAM value of 0.493 degrees decreased compared to BM's KAM value.
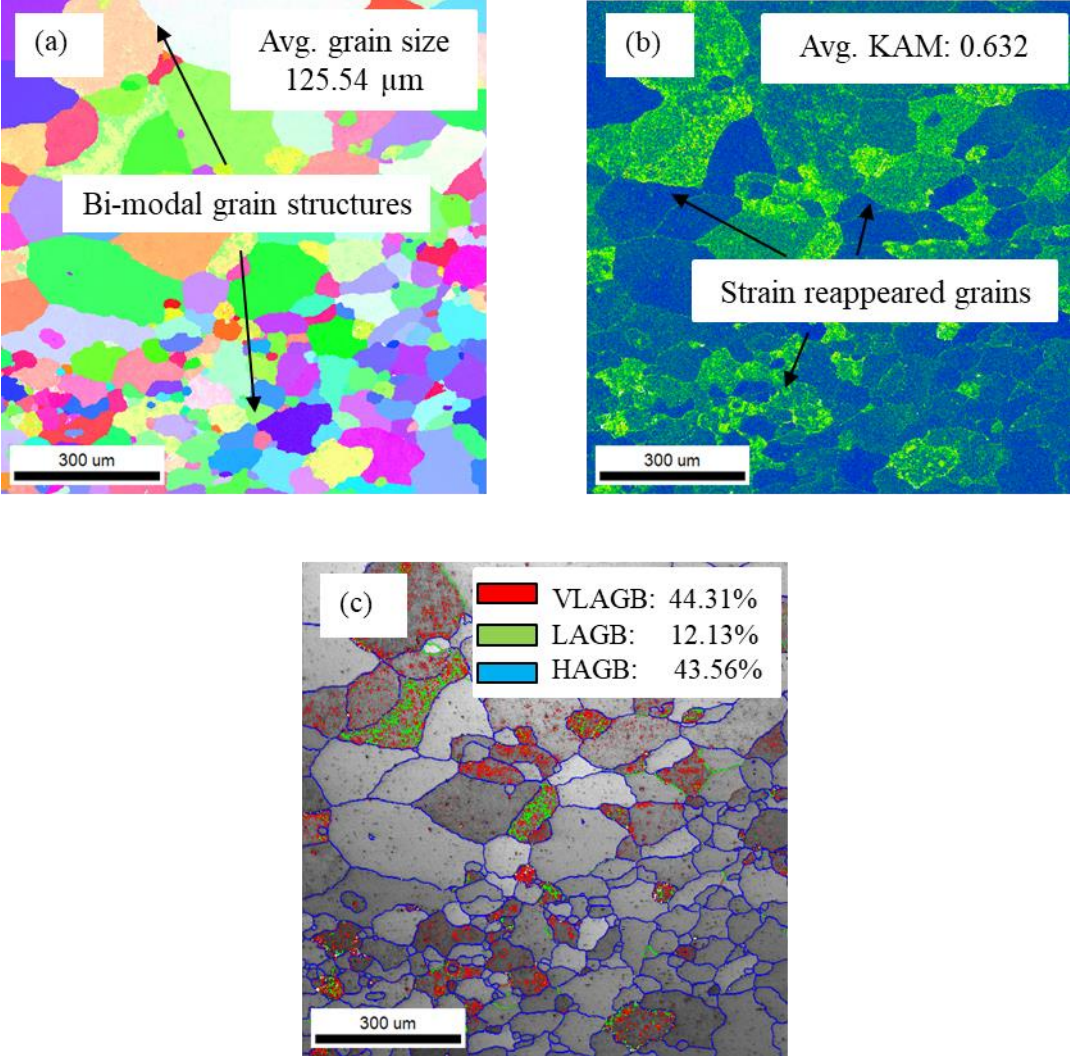
Figure 3.5 EBSD analysis: (a) IPF map, (b) KAM map, (c) GBCD map in the SZ of the PWHT joint.

Figure 3.5(a-c) revealed the microstructural characterization SZ of the PWHT joint. The IPF and GBCD maps of the SZ demonstrated the abnormal grain growth phenomenon, drastically increasing the average grain sizes of 125.54 μm, as exhibited in Figure 3.5(a, c). AGG is a phenomenon that occurs when a number of grains in a material grow much larger than the surrounding grains. The material in the SZ is subjected to severe plastic deformation and dynamic recrystallization during the FSW, creating ultrafine grains with high-angle grain

boundaries (HAGBs) and substructures such as dislocations and deformation bands. The immense energy stored within these highly deformed and recrystallized grains serves as the place for nucleation for abnormal grain growth after heat treatment, generating enormous grains that are significantly larger than the neighboring grains. AGG phenomena in the SZ can negatively impact the material's mechanical properties. The larger grains resulting from abnormal grain growth can act as weak spots in the material, reducing strength and ductility. In addition, larger grains tend to have lower dislocation densities and fewer grain boundaries than smaller grains, making them more prone to deformation and failure. Moreover, larger grains may have various crystallography orientations and react to external forces differently, which can also cause anisotropy in the characteristics of the SZ. AGG phenomena can also result in a non-uniform grain size distribution, which impacts a material's overall characteristics and the homogeneity of its microstructure [25,26]. Additionally, after heat treatment, a significant increase was observed in the proportion of LAGBs in the stir zone, with a percentage of 56.4%, as exhibited in Figure 3.5(c). However, most LAGBs were located inside large grains. Furthermore, with the aid of KAM maps, as shown in Figure 3.5(b), subgrains were found in the grain interiors. The average KAM value increased after heat treatment in SZ to 0.632 degrees. Sub-grains are small regions within a grain that exhibit slightly different crystallographic orientations from the other parts. PWHT involves subjecting a material to high temperatures, in which atomic movement is activated, leading to the diffusion and annihilation of these defects and restoring the crystal lattice. Sub-grains are formed due to dislocation slip and rearrangement of dislocation networks, which also cause the formation of small misorientation boundaries within grains [27]. In addition, the stir zone typically exhibits a bimodal microstructure, which consists of two distinct regions from diverse grain sizes. A bimodal structure can occur due to coarse continuous static recrystallization (CSRX) grains and fine discontinuous static recrystallization (DSRX) grains. The migration and coalescence of LAGBs in CSRX result in subgrain coarsening. A moving sub-

boundary absorbs dislocations, increasing misorientation and energy, eventually transforming the LAGBs into HAGBs. As a result, subgrains bounded by LAGBs, produced by static recovery (SRV), are continuously replaced by subgrains and, subsequently, grains delimited by HAGBs from all sides. In DSRX, the recrystallization mechanism involves the migration of HAGBs, nucleation of new grains at bulging caps, and subsequent growth of recrystallized grains [27]. The process is driven by energy considerations, balancing the decrease in energy from dislocation consumption with the increase in energy from increased grain boundary area. The resulting microstructure is often heterogeneous, with varying grain sizes and orientations and a bimodal particle size distribution. A bimodal structure is established in the SZ by existing simultaneously in these two populations of grains [28,29,30]. The presence of a bimodal structure might affect the material's mechanical characteristics in a beneficial as well as detrimental manner. On the positive side, the bimodal structure can improve strength and ductility, allowing for more efficient load transfer between the larger and smaller grains. The smaller grains can act as obstacles to dislocation motion, leading to increased strength, while the larger grains can act as deformation zones, leading to increased ductility. On the negative side, the bimodal structure can also reduce the material's fatigue life, as the presence of two distinct grain sizes can create stress concentration points and promote crack initiation. It is important to note that having a bimodal structure can cause uneven deformation during processing.

3.2. Mechanical properties

The strength of the BM, FSW, and PWHT joints was compared using the engineering stress strain graphs, as given in Figure 3.6. The ultimate tensile strength of the FSW joint decreased significantly in relation to the BM, although enhancement of elongation was observed from 21% to 29%. In addition, joint yield strength decreased over three times after the FSW process, from 322.7 MPa to 105.3 MPa. During the post-weld heat treatment, mechanical properties showed a contrasting tendency. Notably, the ultimate strength and yield strength increased to 287.8 MPa

and 264.2 MPa, respectively, while the elongation decreased by 6.2% and 14.2% compared to the BM and as welded, respectively, as denoted in Table 3.1. Furthermore, the stress strain curve of the FSW joint is characterized by sudden load drops that correspond until another burst of deformation occurs, known as the PLC (Portevin-Le Chatelier) effect, a complex phenomenon that takes place during plastic deformation in metallic materials [31]. The most notable characteristic of this phenomenon is the appearance of a serrated flow pattern, which is attributed to a series of intermittent jumps in the stress required for plastic deformation. The root causes of the PLC effect are believed to be related to dynamic strain aging, a phenomenon caused by the interaction of dislocations and solute atoms. Specifically, solute atoms are attracted to dislocations and can pin them in place, requiring a more significant force to break them free [32]. Dislocations can move at a lower stress than required to start the deformation if an area of the material starts deforming and becomes free of solute atoms. A band that spans the entire specimen forms when the deformation travels to nearby locations. The solutes may diffuse to different dislocations during the band's propagation, trapping them in position. As a result, greater power is required to begin plastic deformation again [33,34]. However, this phenomenon is no longer visible in the PWHT joint's stress strain curve. During PWHT, the material goes through a number of thermally stimulated processes, including recovery, recrystallization, and grain growth, which boost dislocation elimination and solve atom diffusion away from the dislocations. This method minimizes the likelihood of dynamic strain aging and removes the serrated flow pattern in a stress-strain curve [15,35].

Surface microhardness mapping (2D) and the microhardness profile via the centerline on the surface of the FSW and PWHT joints cross-sections were performed, as shown in Figure 3.7. The softening impact seen in the SZ and TMAZ following the FSW resulted in a significant drop in the microhardness profile, from around 115.8 HV (base metal) to a value of about 58.8 HV. However, during PWHT, not only has homogeneous microhardness been observed, but

there has also been an increase in all zones. Specifically, a significant increase in microhardness was witnessed from 104.4 HV to 114.2 HV. This improvement is attributed to the re-precipitation of the secondary phase dispersoid.

Table 3.1 Mechanical properties of the BM, FSW, and PWHT joints.

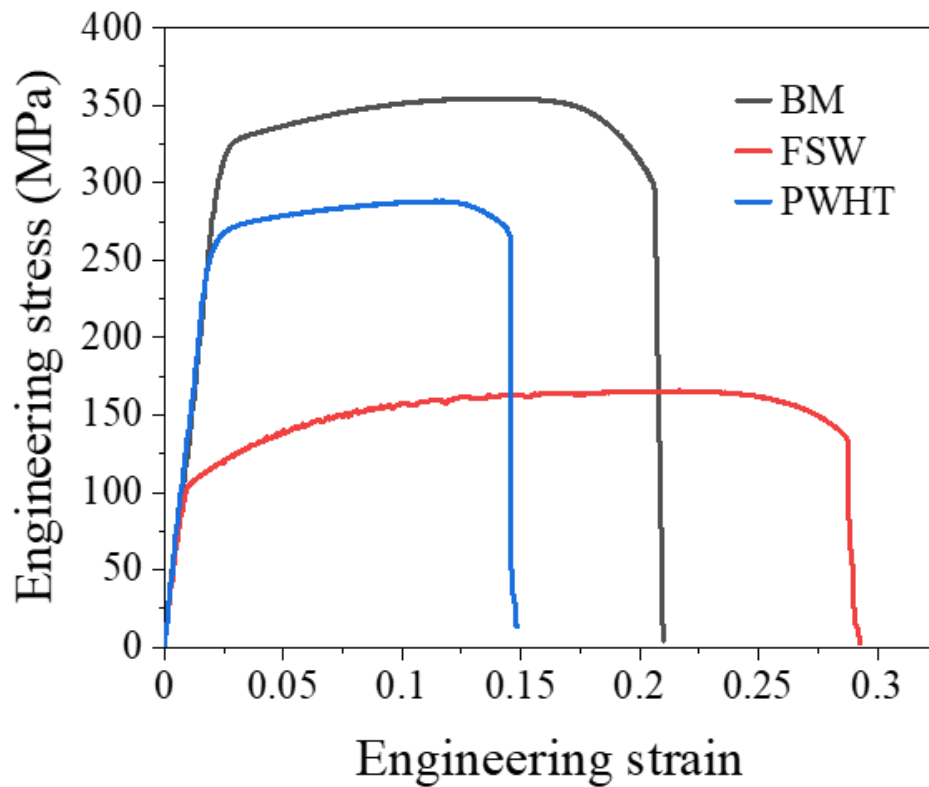| Materials	Yield strength (MPa)	Ultimate tensile strength (UTS, MPa)	Elongation (%)
BM	322.7	354.2	21.0
FSW	105.3	165.1	29.0
PWHT	264.2	287.8	14.8

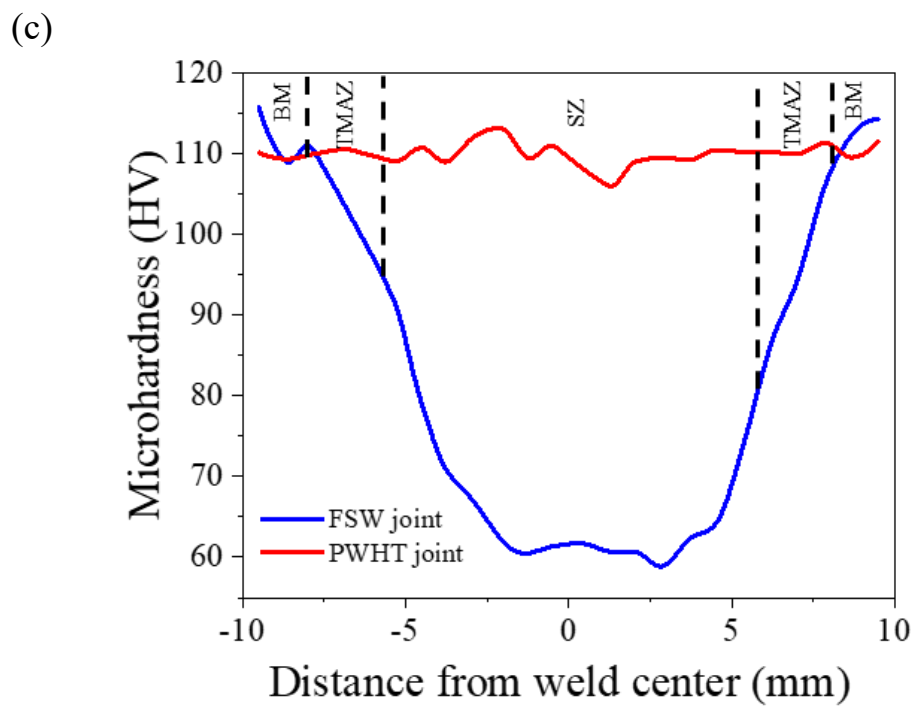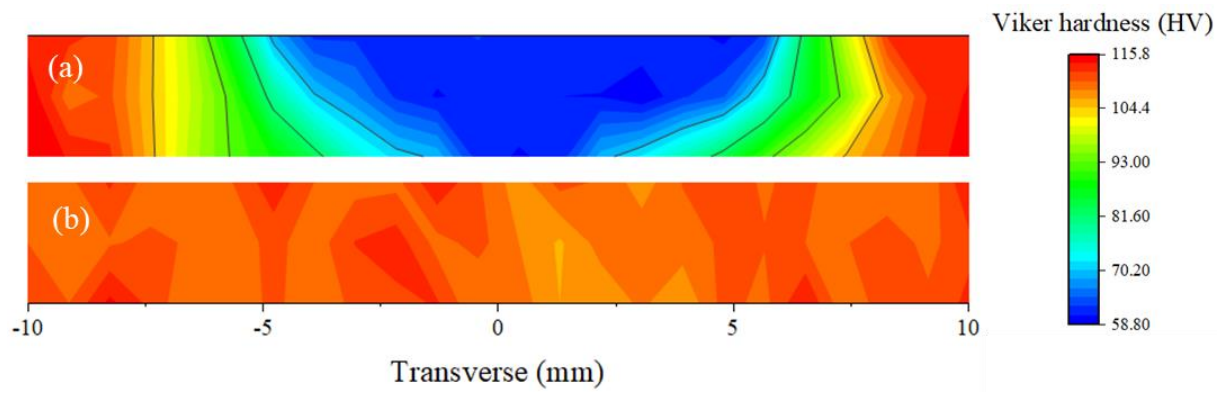Figure 3.6 Stress-strain curves of the base metal, FSW, and PWHT joints.

Figure 3.7 Microhardness mapping of (a) the FSW joint and (b) PWHT; (c) microhardness profile of weld cross-section
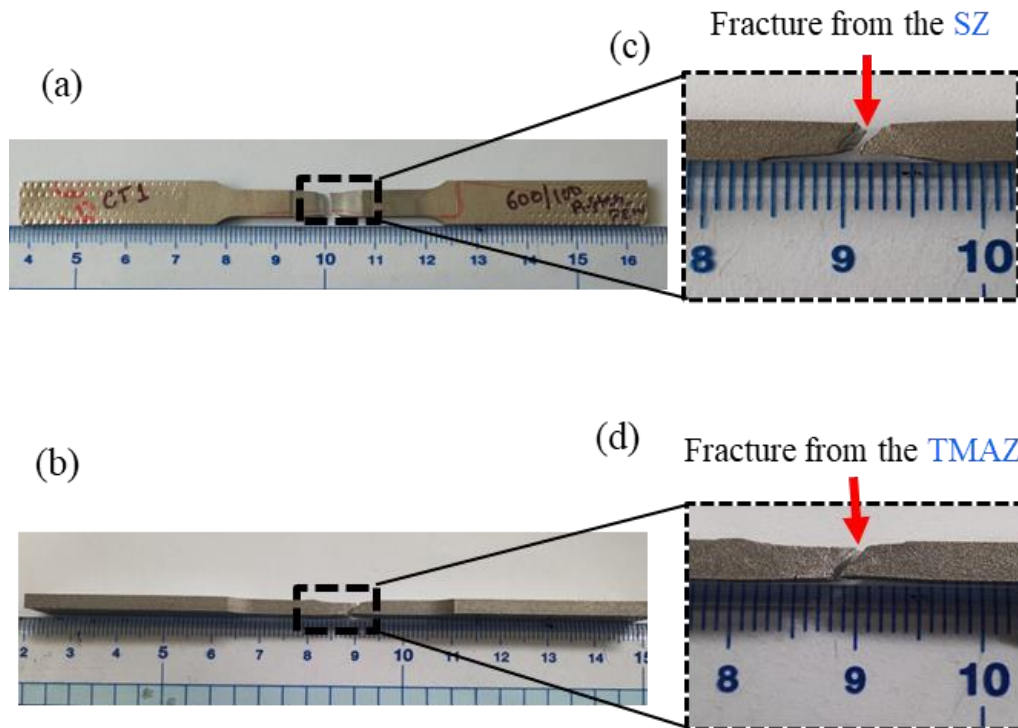
Figure 3.8 The broke tensile specimens fractured visual position in (a) the FSW and (b) the PWHT joints; (c, d) magnified views of the rupture area of (a, b).

The FSW and PWHT joints are fractured at different positions, as shown in Figure 3.8. In the FSW joint, the fracture is observed at SZ (Figure 3.8(a)), while the PWHT joint is fractured at the TMAZ, as displayed in Figure 3.8(b). The morphology of the fracture FSW transverse tensile specimens was examined to determine the fracture mechanism, as illustrated in Figure 3.9(a, c). The fracture surface exhibited variable size and depth dimples, indicating that the material underwent significant plastic deformation before fracture, leading to micro-void formation. The dimples are formulated due to the formation and coalescence of these voids, leading to a rough fracture surface. Furthermore, the dimples on the fracture surface were displayed in both the PWHT and FSW joints, as shown in Figure 3.9(b, d), which indicated a ductile mode of failure.
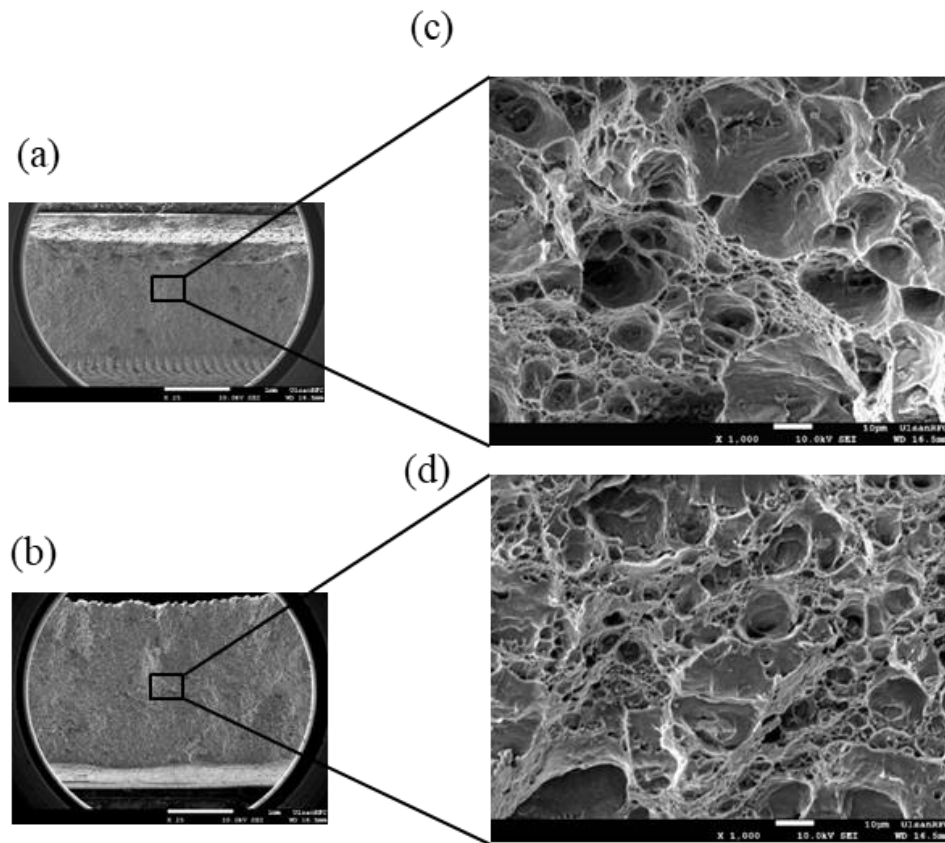
Figure 3.9 (a, b) SEM fractography of the fractured tensile specimens in the FSW and the PWHT joints; (c, d) magnified views of the areas in (a) and (b) that are indicated by black rectangles.

4. CONCLUSION

In this present study, the effect of post-weld heat treatment on AA6061-T6 was elucidated through microstructural analysis and mechanical testing. The most significant conclusions are summarized below:

(1) PWHT showed significant microstructural changes and the recovery of mechanical properties from the FSW joint.

(2) The results of SEM-EDS analysis suggested that re-precipitates were produced during PWHT, which concentrated at the grain boundary and grain boundary junction.

(3) IPF, KAM, and GBCD maps revealed an average grain size of up to 125.54 µm, sub-grain development, the existence of abnormal growth grain phenomenon, and bimodal grain structure in the stir zone following PWHT.

(4) Mechanical properties of the PWHT joint showed a significant enhancement, particularly an increase in tensile strength and microhardness.

(5) The fracture surfaces observed in the TMAZ of PWHT and SZ of the FSW joint exhibited the presence of dimples, indicating a ductile mode of failure.

REFERENCE

1   Taub, A., De Moor, E., Luo, A., Matlock, D. K., Speer, J. G., & Vaidya, U. (2019). Materials for Automotive Lightweighting. Annual Review of Materials Research, 49, 327–359. https://doi.org/10.1146/annurev-matsci-070218-010134.

2   Zhang, W., & Xu, J. (2022). Advanced lightweight materials for Automobiles: A review. In Materials and Design (Vol. 221). ElsevierLtd, https://doi.org/10.1016/j.matdes.2022.110994.

3   Dubey, R., Jayaganthan, R., Ruan, D., Gupta, N. K., Jones, N., & Velmurugan, R. (2023). Energy absorption and dynamic behaviour of 6xxx series aluminium alloys: A review. International Journal of Impact Engineering, 172, 104397. https://doi.org/https://doi.org/10.1016/j.ijimpeng.2022.104397.

4   Madgule, M., Sreenivasa, C. G., & Borgaonkar, A. V. (2023). Aluminum metal foam production methods, properties, and applications- a review. Materials Today: Proceedings, 77, 673–679, https://doi.org/https://doi.org/10.1016/j.matpr.2022.11.287.

5   Zhang, Y. M., Yang, Y. P., Zhang, W., & Na, S. J. (2020). Advanced Welding Manufacturing: A Brief Analysis and Review of Challenges and Solutions. Journal of Manufacturing Science and Engineering, Transactions of the ASME, 142(11), https://doi.org/10.1115/1.4047947.

6   Mishra, R. S., & Ma, Z. Y. (2005). Friction stir welding and processing. In Materials Science and Engineering R: Reports (Vol. 50, Issues 1–2), https://doi.org/10.1016/j.mser.2005.07.001.

7   Singh, R., Dubey, S., Singh, A., & Kumar, S. (2020). A review paper on friction stir welding process. Materials Today: Proceedings, 38, https://doi.org/10.1016/j.matpr.2020.05.208.

8   Basak, S., Mondal, M., Gao, K., Hong, S. T., Anaman, S. Y., & Cho, H. H. (2022). Friction stir butt-welding of roll cladded aluminum thin sheets: effect of microstructural and texture changes on mechanical properties. Materials Science and Engineering A, 832. https://doi.org/10.1016/j.msea.2021.142490.

9   Zhang, L., Zhong, H., Li, S., Zhao, H., Chen, J., & Qi, L. (2020). Microstructure, mechanical properties and fatigue crack growth behavior of friction stir welded joint of 6061-T6 aluminum alloy—International Journal of Fatigue, 135, 105556, https://doi.org/10.1016/j.ijfatigue.2020.105556.

10 Zhang, Y., Chen, X., Li, Z., & Yang, Z. (2021). Effect of high rotational-speed friction-stir welding on microstructure and properties of welded joints of 6061-T6 alloy ultrathin plate. Materials, 14(20). https://doi.org/10.3390/ma14206012.

11 Choi, W. J., Morrow, J. D., Pfefferkorn, F. E., & Zinn, M. R. (2017). The Effects of Welding Parameters and Backing Plate Diffusivity on Energy Consumption in Friction Stir Welding. Procedia Manufacturing, 10, 382–391, https://doi.org/10.1016/j.promfg.2017.07.011.

12 Fratini, L., Buffa, G., & Shivpuri, R. (2010). Mechanical and metallurgical effects of in process cooling during friction stir welding of AA7075-T6 butt joints. Acta Materialia, 58(6), 2056–2067, https://doi.org/10.1016/j.actamat.2009.11.048.

13 Heurtier, P., Jones, M. J., Desrayaud, C., Driver, J. H., Montheillet, F., & Allehaux, D. (2006). Mechanical and thermal modelling of Friction Stir Welding, Journal of Materials Processing Technology, 171(3), 348–357. https://doi.org/https://doi.org/10.1016/j.jmatprotec.2005.07.014.

14 Rajendran, C., Srinivasan, K., Balasubramanian, V., Balaji, H., & Selvaraj, P. (2016). Influences of post weld heat treatment on tensile strength and microstructure characteristics of friction stir welded butt joints of AA2014-T6 aluminum alloy. 25(3–4), 89–98, https://doi.org/doi:10.1515/jmbm-2016-0011.

15 Baghdadi, A. H., Rajabi, A., Selamat, N. F. M., Sajuri, Z., & Omar, M. Z. (2019). Effect of post-weld heat treatment on the mechanical behavior and dislocation density of friction stir welded Al6061. Materials Science and Engineering A, 754, 728–734, https://doi.org/10.1016/j.msea.2019.03.017.

16 Ipekoglu, G., Erim, S., & Cam, G. (2014). Investigation into the influence of post-weld heat treatment on the friction stir welded AA6061 Al-Alloy plates with different temper conditions. Metallurgical and Materials Transactions A: Physical Metallurgy and Materials Science, 45(2), 864–877, https://doi.org/10.1007/s11661-013-2026-y.

17 Pabandi, H. K., Jashnani, H. R., & Paidar, M. (2018). Effect of precipitation hardening heat treatment on mechanical and microstructure features of dissimilar friction stir welded AA2024-T6 and AA6061-T6 alloys. Journal of Manufacturing Processes, 31, 214–220, https://doi.org/10.1016/j.jmapro.2017.11.019.

18 Momeni, M., & Guillot, M. (2018). Development of friction stir welding technique at right angle (RAFSW) applied on butt joint of AA6061-T6 aluminum alloy. International Journal of Advanced Manufacturing Technology, 99(9–12), 3077–3089, https://doi.org/10.1007/s00170-018-2672-8.

19 Gladman, T. (1999). Precipitation hardening in metals. Materials Science and Technology, 15(1), 30–36. https://doi.org/10.1179/026708399773002782.

20 Pashley, D. W., Jacobs, M. H., & Vietz, J. T. (1967). The basic processes affecting two-step ageing in an Al-Mg-Si alloy. The Philosophical Magazine: A Journal of Theoretical Experimental and Applied Physics, 16(139), 51–76, https://doi.org/10.1080/14786436708229257.

21 Zhao, B. M., Hu, M., Zhu, J., Han, Z. Y., Sun, H. Q., & Ji, Y. L. (2018). Study on Two-Step Aging Technology of 6082 Aluminum Bumper. Key Engineering Materials, 764, 245–251, https://doi.org/10.4028/www.scientific.net/KEM.764.245.

22 Dong, P., Li, H., Sun, D., Gong, W., & Liu, J. (2013). Effects of welding speed on the microstructure and hardness in friction stir welding joints of 6005A-T6 aluminum alloy, Materials & Design, 45, 524–531, https://doi.org/https://doi.org/10.1016/j.matdes.2012.09.040.

23 Kim, I., Song, M., & Kim, J. (2021). Nanocluster formation and two-step aging behavior in Al–Mg–Si(-xCu: X = 0–4 mass%) alloys. Journal of Alloys and Compounds, 857, 157596, https://doi.org/https://doi.org/10.1016/j.jallcom.2020.157596.

24 Yang, Z., & Banhart, J. (2021). Natural and artificial ageing in aluminium alloys – the role of excess vacancies. Acta Materialia, 215, 117014, https://doi.org/10.1016/j.actamat.2021.117014.

25 Attallah, M. M., & Salem, H. G. (2005). Friction stir welding parameters: a tool for controlling abnormal grain growth during subsequent heat treatment. Materials Science and Engineering: A, 391(1), 51–59, https://doi.org/https://doi.org/10.1016/j.msea.2004.08.059.

26 Vysotskiy, I., Malopheyev, S., Mironov, S., & Kaibyshev, R. (2018). Pre-strain rolling as an effective tool for suppression of abnormal grain growth in friction-stir welded 6061 aluminum alloy. Materials Science and Engineering: A, 733, 39–42, https://doi.org/https://doi.org/10.1016/j.msea.2018.07.026.

27 Heidarzadeh, A., Mironov, S., Kaibyshev, R., Çam, G., Simar, A., Gerlich, A., Khodabakhshi, F., Mostafaei, A., Field, D., Robson, J., Deschamps, A., & Withers, P. (2020). Friction stir welding/processing of metals and alloys: A comprehensive review on microstructural evolution. Progress in Materials Science.

28 Liu, F., Zhao, H., & Xu, Z. (2022). Effect of post-weld heat treatment on the microstructure and mechanical properties of SSFSW HVDC AlSiMgMnCu alloy. Journal of Materials Research and Technology, 21, 3686–3702. https://doi.org/https://doi.org/10.1016/j.jmrt.2022.11.012.

29 Han, G., Lee, K., Yoon, J.-Y., Na, T.-W., Ahn, K., Kang, M.-J., & Jun, T.-S. (2021). Effect of post-weld heat treatment on mechanical properties of local weld-affected zones in friction stir welded AZ31 plates. Materials Science and Engineering: A, 805, 140809, https://doi.org/https://doi.org/10.1016/j.msea.2021.140809.

30 Kalinenko, A., Mishin, V., Shishov, I., Malopheyev, S., Zuiko, I., Novikov, V., Mironov, S., Kaibyshev, R., & Semiatin, S. L. (2022). Mechanisms of abnormal grain growth in friction-stir-welded aluminum alloy 6061-T6. Materials Characterization, 194, 112473, https://doi.org/https://doi.org/10.1016/j.matchar.2022.112473.

31 Cetlin, P. R., Güleç, A. Ş., & Reed-Hill, R. E. (1973). Serrated flow in aluminum 6061 alloy. Metallurgical Transactions, 4(2), 513–517. https://doi.org/10.1007/BF02648704.

32 Robinson, J. M., & Shaw, M. P. (1994). Microstructural and mechanical influences on dynamic strain aging phenomena. International Materials Reviews, 39(3), 113–122. https://doi.org/10.1179/imr.1994.39.3.113.

33 Yilmaz, A. (2011). The Portevin–Le Chatelier effect: a review of experimental findings. Science and Technology of Advanced Materials, 12(6), 063001.

    https://doi.org/10.1088/1468-6996/12/6/063001

34 Zhang, P., Liu, G., & Sun, J. (2022). A critical review on the Portevin-Le Chatelier effect in aluminum alloys. Journal of Central South University, 29(3), 744–766. https://doi.org/10.1007/s11771-022-4977-x.

35 Han, G., Lee, J.-R., Noh, Y., & Jun, T.-S. (2022). The role of cryogenic quenching on the mechanical properties of FSWed 6061-T6 aluminum alloy. Materials Science and Engineering: A, 840, 142896. https://doi.org/https://doi.org/10.1016/j.msea.2022.142896.